Modelling of dielectric hysteresis loops in ferroelectric semiconductors with charged defects

2004 J. Phys.: Condens. Matter 16 8937

(http://iopscience.iop.org/0953-8984/16/49/010)

INSTITUTE OF PHYSICS PUBLISHING JOURNAL OF PHYSICS: CONDENSED MATTER

J. Phys.: Condens. Matter **16** (2004) 8937–8956 PII: S0953-8984(04)85520-6

Modelling of dielectric hysteresis loops in ferroelectric semiconductors with charged defects

Anna N Morozovska[1] **and Eugene A Eliseev**[2]

[1] V Lashkaryov Institute of Semiconductor Physics, NAS of Ukraine, 45, pr. Nauki, 03028 Kiev, Ukraine
[2] Institute for Problems of Materials Science, National Academy of Science of Ukraine, Krjijanovskogo 3, 03142 Kiev, Ukraine

E-mail: morozo@i.com.ua and eliseev@i.com.ua

Received 30 August 2004
Published 26 November 2004
Online at stacks.iop.org/JPhysCM/16/8937
doi:10.1088/0953-8984/16/49/010

Abstract

We have proposed the phenomenological description of dielectric hysteresis loops in ferroelectric semiconductors with charged defects and prevailing extrinsic conductivity. We have modified the Landau–Ginsburg approach and shown that the macroscopic state of the aforementioned inhomogeneous system can be described by three coupled equations for three order parameters. Both the experimentally observed coercive field values well below the thermodynamic values and the various hysteresis-loop deformations (constricted and double loops) have been obtained in the framework of our model. The obtained results quantitatively explain the ferroelectric switching in such ferroelectric materials as thick PZT films.

(Some figures in this article are in colour only in the electronic version.)

1. Introduction

The spontaneous electric displacement switching under an external field is one of the essential features of ferroelectric materials [1, 2]. The main comprehensively studied characteristics of a ferroelectric hysteresis loop are the spontaneous displacement and coercive field values [2, 3]. However, conventional theoretical approaches give a significantly incomplete picture of the displacement switching, namely:

- Nucleation theory [4] proved that the ferroelectric inhomogeneities promote the nucleation of domains, the appearance of several nuclei in the ferroelectric film does not need to overcome the energetic barrier due to the long range interaction between them [5]. The calculated value of the coercive field is inversely proportional to the film thickness [6] and thus nucleation theory can explain the drastic increase of the coercive field with the decrease in film thickness experimentally observed in some thin films [7, 8]. However, nucleation theory predicts that

the coercive field tends to zero with increase in film thickness and this theory seems unsuitable for thick films and bulk materials.

- The domain kinetics theory evolved in [9, 10] uses the Kolmogorov–Avrami statistical model (see chapter 4 in [11]). It allows one to describe experimental data with high accuracy due to the great amount of fitting parameters without clear interpretation. The obtained results themselves represent only computer simulations.
- The Landau–Ginsburg theory (see [3], and also chapter 7 in [11]) evolved for the mono-domain perfect ferroelectrics describes so-called homogeneous switching without domains. This theory cannot describe domain pinning, domain nucleation and domain wall movement. Calculated values of the thermodynamic coercive field [2, 3] are from several times to several orders greater than the experimentally observed values for the real bulk ferroelectric materials (see e.g. [12, 13]). Renormalized Landau–Ginsburg free energy with coefficients depending on the film thickness and boundary conditions characteristics [14, 15] does not describe adequately ferroelectric hysteresis even in epitaxial film, because it predicts very sharp coercive field relaxation up to the aforementioned thermodynamic coercive field with film thickness increase [16].
- As for the imperfect doped ferroelectrics, here the hysteresis loops look much thinner [17–20] than Landau–Ginsburg ones, and its shape undergoes various deformations ('slim' loops [21], chapter 5 in [12]; minor loops [22, 23]; constricted loops [24, 25]). Therefore, the modification of Landau–Ginsburg free energy (and thus Landau–Khalatnikov equation [3] derived from it by variational method) suitable for the description of inhomogeneous ferroelectrics switching seems necessary. Incorporation of the modified free energy with contribution from inhomogeneities could be a solution to this problem.

To our mind, the inhomogeneous electric fields caused by charged defects should be taken into account. However, in contrast to the random field theory, developed for the relaxor insulator ferroelectrics [26], semiconductor properties of these materials [27] (at least extrinsic conductivity created by charged impurities [28, 29]) should be taken into consideration. Right in the way we modified the Landau–Ginsburg approach for the ferroelectric-semiconductors with charged defects and found both the essential coercive field decrease and the hysteresis-loops' deformation experimentally observed in inhomogeneous systems.

2. The problem

The majority of imperfect ferroelectrics with non-isovalent impurities or some unavoidable imperfections would be considered rather as extrinsic semiconductors [27, 28] than perfect insulators.

We assume that almost immovable non-stochiometric defects or non-isovalent impurity centres are embedded into hypothetical perfect uniaxial ferroelectric (the z direction coincides with the polar axis). We suppose that impurity centres or defects are ionized (e.g. after UV, photo- or thermal excitation) and even in the absence of proper conductivity, they provide a prevailing extrinsic conductivity in the bulk sample.

For the sake of simplicity, we regard that the sample as a whole is the electro-neutral n-type extrinsic semiconductor with positively charged defects with density $\rho_s(\mathbf{r})$. The microscopic spatial distribution of these defects' charge density $\rho_s(\mathbf{r})$ is characterized by the average charge density $\bar{\rho}_s$ proportional to the ionized defects' concentration and microscopic modulation $\delta\rho_s$, i.e. $\rho_s(\mathbf{r}) = \bar{\rho}_s + \delta\rho_s(\mathbf{r})$. The modulation $\delta\rho_s$ fluctuates due to the great variety of misfit effects (lattice distortions, local shift, possible clusterization at high defect concentration).

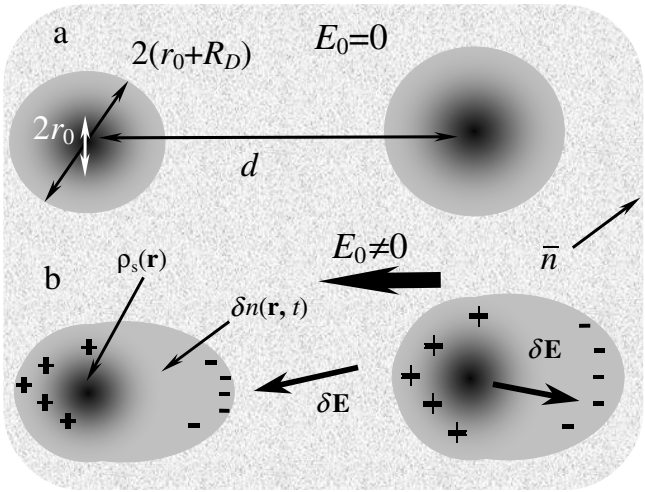

Scheme 1. Charged defects with the charge density ρ_s (dark circles with radius r_0) are screened by the free charges with density δn (grey circles or ellipses with screening radius R_D). (a) and (b) show the system with the zero and non-zero external field E_0 respectively.

For the sake of simplicity, let us assume that charged defects' spatial distribution is quasi-homogeneous, i.e. the average distance between defects $d \cong a/\sqrt[3]{n_d}$ (a is the lattice constant and n_d is the defect concentration). The size distribution function of charged defects is well localized near its sharp maximum at the average size $2r_0$.

The movable screening clouds $\delta n(\mathbf{r}, t)$ surround each charged centre (see scheme 1(a)). The characteristic size of these screening clouds is of the same order as the Debye screening radius R_D. When one applies the external field E_0, screening clouds of free charges are deformed, and nano-system 'defect centre + screening cloud' becomes polarized (scheme 1(b)). Polarized regions '$\delta\rho_s(\mathbf{r}) + \delta n(\mathbf{r}, t)$' cause the additional inner electric field fluctuations $\delta E(\mathbf{r}, t)$. According to the equations of state, the fluctuations of the inner electric field δE cause displacement fluctuations δD.

3. General equations

Hereinafter we assume that the period of changing of the external field is much greater than the free carriers' relaxation time, and therefore the quasi-static approximation $\mathrm{rot}\,\mathbf{E} = 0, \mathrm{rot}\,\mathbf{H} = 0$ is valid. Thus, Maxwell's equations for the quasi-static electric field $\mathbf{E}$ and displacement D have the form:

$$\mathrm{div}\,\mathbf{D} = 4\pi\rho, \qquad \frac{\partial \mathbf{D}}{\partial t} + 4\pi\mathbf{j}_c = 0. \tag{1}$$

They have to be supplemented by the material expressions for current and charge density:

$$\mathbf{j}_c = \sum_m (\mu_m \rho_m \mathbf{E} - \kappa_m\,\mathrm{grad}\,\rho_m), \qquad \rho(\mathbf{r}, t) = \sum_m \rho_m(\mathbf{r}, t) + \rho_s(\mathbf{r}). \tag{2}$$

Here ρ_m, μ_m and κ_m are the m-type movable charge volume density ($m = n, p$), mobility and diffusion coefficient respectively, $\mathbf{j}_c$ is the macroscopic free-carriers' current, $\rho_s(\mathbf{r})$ is the fluctuating charge density of static defects.

Keeping in mind that the sample is the extrinsic semiconductor with prevailing n-type conductivity, hereinafter we neglect the proper conductivity, put $n \approx \sum_m \rho_m$ and omit the subscript 'm'. So equations (1), (2) can be rewritten as

$$\operatorname{div} \mathbf{D} = 4\pi(n + \rho_s), \qquad \mu n \mathbf{E} - \kappa \operatorname{grad} n + \frac{1}{4\pi}\frac{\partial}{\partial t}\mathbf{D} = 0. \tag{3}$$

Here $n < 0, \mu < 0$ and $\kappa > 0$. In accordance with Einstein relation $\mu/\kappa \approx e/k_B T^*$ ($e < 0$) the Debye screening radius $R_D = \sqrt{\kappa/4\pi n\mu} \approx \sqrt{|k_B T^*/4\pi n e|}$ [27, 28]. Hereafter we suppose that the homogeneous external field $E_0(t)$ is applied along the polar z-axis. The sample is infinite in the transverse directions. It is rather thick and its boundaries $z = -1$ and $z = 1$ are equivalent. We suppose that the potentials of electrodes are given, so that the inner field satisfies the condition:

$$\frac{1}{2\ell}\int_{-\ell}^{\ell} E_z(\mathbf{r}, t)\, \mathrm{d}z = E_0(t). \tag{4}$$

Hereinafter we introduce the averaging over sample volume V:

$$f(\mathbf{r}, t) = \overline{f(t)} + \delta f(\mathbf{r}, t), \qquad \overline{f}(t) = \frac{1}{V}\int_V f(\mathbf{r}, t)\, \mathrm{d}\mathbf{r}. \tag{5}$$

Hereinafter the dash designates the averaging of functions $f = \{n, \rho_s, E, D\}$, by definition $\overline{\delta f(\mathbf{r}, t)} = 0$. The spatial distribution of the deviations $\delta f(\mathbf{r}, t)$ consists of the part caused by spontaneous displacement screening [27] and localized in the ultrathin screening surface regions [30] and the one caused by microscopic modulation $\delta\rho_s$ with quasi-homogeneous spatial distribution. For the μm-thick sample the contribution from the ultrathin screening region to the average functions is negligibly small, and the averaging over sample volume is equivalent to the statistical averaging with homogeneous distribution function. Using this distribution function properties, one can regard that

$$\overline{\delta f^{2m+1}(\mathbf{r}, t)} \approx 0, \qquad m = 1, 2, \ldots, \tag{6}$$

and the correlation between the different δf-functions is equal to zero if the total power of the functions is an odd number.

It follows from (3)–(5) that

$$\mathbf{D}(\mathbf{r}, t) = \mathbf{e}_z \overline{D(t)} + \delta\mathbf{D}(\mathbf{r}, t), \tag{7a}$$

$$\mathbf{E}(\mathbf{r}, t) = \mathbf{e}_z E_0(t) + \delta\mathbf{E}(\mathbf{r}, t). \tag{7b}$$

Here $\mathbf{e}_z$ is the unit vector directed along the z-axis, $\overline{E}$ is the applied uniform field $E_0(t)$ and $\overline{E}_{x,y} = 0$. Note that the average values $\overline{E}$, $\overline{D}$ are determined experimentally [1–3]. Having substituted (7) into (3) and averaged, one can obtain the expressions for the average quantities, namely:

$$\bar{n} = -\bar{\rho}_s, \qquad \mu\bar{n}E_0 + \mu\,\overline{\delta n\, \delta E_z} + \frac{\partial}{\partial t}\frac{\overline{D}(t)}{4\pi} = 0, \qquad \mu\,\overline{\delta n\, \delta E_{x,y}} = 0. \tag{8}$$

Absence of the average space charge density $\bar{\rho}$ follows from the sample electro-neutrality. Using $\rho_s = \bar{\rho}_s + \delta\rho_s$ and $n = \bar{n} + \delta n$ in (7) and (8) one can obtain from (3) that

$$\operatorname{div}(\delta\mathbf{D}) = 4\pi(\delta n + \delta\rho_s(\mathbf{r})), \tag{9}$$

$$\mu(\delta n\, E_0\mathbf{e}_z - \bar{\rho}_s\, \delta\mathbf{E}) + \mu(\delta n\, \delta\mathbf{E} - \overline{\delta n\, \delta\mathbf{E}}) - \kappa \operatorname{grad} \delta n + \frac{1}{4\pi}\frac{\partial}{\partial t}\delta\mathbf{D} = 0. \tag{10}$$

The term $\mu(\delta n\, \delta\mathbf{E} - \overline{\delta n\, \delta\mathbf{E}})$ in (10) can be interpreted as the fluctuating circular electric currents around charged defects, which do not contribute to the average macroscopic current.

As the equation of state, we use the Landau–Khalatnikov equation for the displacement z-component relaxation, but take into account the influence of fluctuating electric field δE_z created by charged defects and correlation effects. This approach takes into consideration the spatial–temporal dispersion of the ferroelectric material. Using the original approach evolved in paper [31] and formula (7), we modify the classical Landau–Khalatnikov equation $\Gamma\partial D_z/\partial t + \alpha D_z + \beta D_z^3 = E_z$ and obtain the following system of coupled equations:

$$\Gamma\frac{\partial \overline{D}}{\partial t} + (\alpha + 3\beta\,\overline{\delta D^2})\overline{D} + \beta\overline{D}^{\,3} = E_0(t), \tag{11}$$

$$\Gamma\frac{\partial}{\partial t}\delta D + (\alpha + 3\beta\overline{D}^2)\delta D + 3\beta\overline{D}(\delta D^2 - \overline{\delta D^2}) + \beta\,\delta D^3 - \gamma\frac{\partial^2 \delta D}{\partial \mathbf{r}^2} = \delta E_z. \tag{12}$$

Here $\Gamma > 0$ is the kinetic coefficient, $\alpha < 0, \beta > 0, \gamma > 0$ are parameters of the hypothetical pure (free of defects) sample. Hereafter we denote $\delta D_z \equiv \delta D$. We would like to emphasize that the sum of equations (11) and (12) coincides with Landau–Khalatnikov equation [3] for D only under the condition $\delta\rho_s = 0$. This condition corresponds to the absence of inhomogeneities or their seeding, and thus only the homogeneous polarization switching can take place when the external field exceeds the thermodynamic coercive field. In such a case, the inner field in the bulk of the sample is the sum of the external field and predetermined depolarization field originated from displacement screening [27]. In contrast to this at $\delta\rho_s \neq 0$ the inner field $\delta\mathbf{E}$ contains the random component dependent on $\delta\rho_s(\mathbf{r})$ and δD in accordance with (9) and (10).

The system of equations (9)–(12) is complete, because the quantities $\delta n, \delta\mathbf{E}$ can be expressed via the fluctuations of displacement δD and $\delta\rho_s(\mathbf{r})$ allowing for (9) and (10). The spatial distribution and temporal evolution of the displacement $\mathbf{D}(\mathbf{r}, t)$ in the bulk sample is determined by the non-linear system (9)–(12) supplemented by the initial distributions of all fluctuating variables (e.g. distribution of charged defects). However, in our opinion, only the implicit numerical schemes adopted for the stochastic differential equations can be used in order to obtain the numerical solutions of (9)–(12). Therefore, hereinafter we consider only the average characteristics of the inhomogeneous ferroelectric semiconductors. The study of the mechanisms of domain wall pinning by the given distribution of charged defects, and domain nucleation during spontaneous displacement reversal is beyond the scope of this paper. Similar problems for the non-conductor ferroelectrics—ideal insulators were considered in detail earlier (see e.g. [32, 33]).

4. Coupled equations

In order to simplify the non-linear system (9)–(12), the following assumption has been used. The charged inhomogeneities are surrounded by screening clouds (see figure 1), therefore $\delta\rho_s \sim \delta n$ and

$$\overline{\delta\rho_s\,\delta n} \approx -\eta\,\overline{\delta\rho_s^2}, \qquad 0 < \eta \ll 1. \tag{13}$$

The small positive function η is determined by the ratio R_D/r_0 (see figure 1 and appendix A).

When the external field amplitude increases, η value slightly decreases due to the polarization of the system 'charged fluctuation + screening cloud'. We suppose that η can be approximated by an effective constant value at not a very high external field.

After elementary transformations of (10), the equation for electric field fluctuation $\delta\mathbf{E}$ acquires the form:

$$\delta\mathbf{E} = \frac{1}{4\pi\mu\bar{\rho}_s}\frac{\partial}{\partial t}\,\delta\mathbf{D} + \mathbf{e}_z\frac{\delta n}{\bar{\rho}_s}E_0(t) - \frac{\kappa}{\mu\bar{\rho}_s}\,\mathrm{grad}\,\delta n + \frac{\delta n\,\delta\mathbf{E} - \overline{\delta n\,\delta\mathbf{E}}}{\bar{\rho}_s}. \tag{14}$$

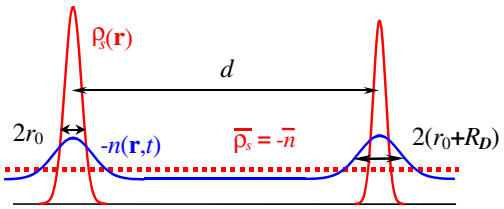

Figure 1. The screening of the charged defects $\delta\rho_s$ by free charges δn at a small amplitude of the external field.

Equation (9) gives

$$\delta n = \frac{1}{4\pi}\,\mathrm{div}(\delta\mathbf{D}) - \delta\rho_s(\mathbf{r}). \tag{15}$$

Using (15) and (14) the electric field fluctuations $\delta\mathbf{E}$ caused by charged defects can be expressed via δD and $\delta\rho_s$:

$$\delta\mathbf{E} \approx \frac{\partial}{\partial t}\frac{\delta\mathbf{D}}{4\pi\mu\bar{\rho}_s} + \left(\mathbf{e}_z E_0(t) - \frac{\kappa\,\mathrm{grad}}{\mu}\right)\left(\frac{\mathrm{div}(\delta\mathbf{D})}{4\pi\bar{\rho}_s} - \frac{\delta\rho_s}{\bar{\rho}_s}\right) + \frac{\overline{\delta\mathbf{E}\,\mathrm{div}(\delta\mathbf{D})} - \delta\mathbf{E}\,\mathrm{div}(\delta\mathbf{D})}{4\pi\bar{\rho}_s} + \frac{\delta\mathbf{E}\,\delta\rho_s - \overline{\delta\mathbf{E}\,\delta\rho_s}}{\bar{\rho}_s}. \tag{16}$$

The equations (11), (12) and (16) comprise the self-consistent system of the non-linear integro-differential equations for δD, δE and $\overline{D}$. Its non-homogeneity is proportional to charge fluctuations $\delta\rho_s$ and external field E_0.

The approximate system of first-order differential equations for average displacement $\overline{D}$, its mean-square fluctuation $\overline{\delta D^2}$ and correlation $\overline{\delta D\,\delta\rho_s}$ can be derived after some elementary transformations of (11), (12) (see [34], appendix B and (13), (16)). Thus, we obtain three coupled equations:

$$\Gamma\frac{\partial\overline{D}}{\partial t} + (\alpha + 3\beta\,\overline{\delta D^2})\overline{D} + \beta\overline{D}^3 = E_0(t), \tag{17a}$$

$$\frac{\Gamma_R}{2}\frac{\partial}{\partial t}\overline{\delta D^2} + (\alpha_R + 3\beta\overline{D}^2)\,\overline{\delta D^2} + \beta(\overline{\delta D^2})^2 = -E_0(t)\frac{\overline{(\delta\rho_s\,\delta D)}}{\bar{\rho}_s} + \vartheta(\overline{\delta\rho_s^2}), \tag{17b}$$

$$\Gamma_R\frac{\partial}{\partial t}\overline{\delta D\,\delta\rho_s} + (\alpha_R + 3\beta\overline{D}^2 + \beta\,\overline{\delta D^2})\,\overline{\delta D\,\delta\rho_s} = -E_0(t)\frac{\overline{\delta\rho_s^2}}{\bar{\rho}_s}\eta. \tag{17c}$$

Here the renormalized coefficients $\alpha_R = \alpha + (\gamma + R_D^2)/d^2$ and $\Gamma_R = \Gamma - 1/4\pi\mu\bar{\rho}_s$ have been introduced. The renormalization of α takes into account the finite value of correlation length and classical renormalization of the gradient term γ by Debye screening radius R_D in the bulk of a sample [30]. The renormalization of Γ takes into account the finite value of the Maxwellian relaxation time $\tau_m = -1/4\pi\mu\bar{\rho}_s$.

The additional source of displacement fluctuations is the term $\vartheta(\overline{\delta\rho_s^2}) = (4\pi R_D)^2(1-\eta)\,\overline{\delta\rho_s^2}$ in the right-hand side of (17*b*). It originates from the diffusion field $\kappa\,\mathrm{grad}(n)/\mu\rho_s$ (see (10), (14) and definition $R_D = \sqrt{\kappa/4\pi n\mu}$). This term has been neglected in the classical equations of Landau–Khalatnikov type as well as in our previous paper [35].

The system (17) determines the temporal evolution of the bulk sample dielectric response and have to be supplemented by the initial values of $\overline{D}$, $\overline{\delta D^2}$ and $\overline{\delta D\,\delta\rho_s}$ at $t = 0$.

Coupled equations (17) have the following physical interpretation (compare with the modified approach [31]). The macroscopic state of the bulk sample with charged defects can be described by three parameters: $\overline{D}$, $\overline{\delta D^2}$ and $\overline{\delta D\,\delta\rho_s}$. The long-range order parameter $\overline{D}$ describes the ferroelectric ordering in the system, and the disorder parameter $\overline{\delta D^2}$ describes disordering caused by inner electric fields caused by charged non-homogeneities $\delta\rho_s$. The correlation $\overline{\delta D\,\delta\rho_s}$ determines the correlations between the movable screening cloud δn and static charged defects $\delta\rho_s$.

We would like to note that the derived system of coupled equations (17) might possess chaotic regions, strange attractors as well as strongly non-ergodic behaviour and continuous relaxation time spectra [11]. Any new system of such a type demands a separate detailed mathematical study that was not the aim of this paper.

5. Ferroelectric hysteresis

In this section, we consider the equilibrium solution of (17), which corresponds to the quasi-static changing external field. Let us demonstrate how the ferroelectric hysteresis loop (i.e. the dependence of displacement $\overline{D}$ over the external field E_0) changes its shape under the presence of charged defects. First, let us rewrite equation (17) in dimensionless variables:

$$\begin{aligned}
&\frac{\mathrm{d}D_m}{\mathrm{d}\tau} - (1 - 3\Delta_D^2)D_m + D_m^3 = E_m,\\
&\frac{\tau_R}{2}\frac{\mathrm{d}\Delta_D^2}{\mathrm{d}\tau} - (\xi - 3D_m^2)\Delta_D^2 + \Delta_D^4 = -E_m K_{D\rho} + gR^2,\\
&\tau_R\frac{\mathrm{d}K_{D\rho}}{\mathrm{d}\tau} - (\xi - 3D_m^2 - \Delta_D^2)K_{D\rho} = -E_m R^2.
\end{aligned} \tag{18}$$

Here, $D_m = \overline{D}/D_S$, $D_S = \sqrt{-\alpha/\beta}$, $E_m = E_0/(-\alpha D_S)$, $\Delta_D = \sqrt{\overline{\delta D^2}}/D_S$, $K_{D\rho} = \overline{\delta D\,\delta\rho_s}/\bar{\rho}_s D_S$, $R^2 = \eta\,\overline{\delta\rho_s^2}/\bar{\rho}_s^2$, $\tau = t/(-\alpha\Gamma)$, $\tau_R = \Gamma/\Gamma_R$ and $g = [(16\pi^2 R_D^2\cdot\bar{\rho}_s^2)/(-\alpha D_S^2)](1-\eta)/\eta$, $\xi = \alpha_R/\alpha$ at $\alpha < 0$.

The renormalized coefficient $\alpha_R = \alpha + (\gamma + R_D^2)/d^2$ is positive and $\alpha_R \gg |\alpha|$ for the typical values of parameters. For example, in $Pb(Zr,Ti)O_3$ in CGSE system, $\gamma \approx 5\times10^{-16}\,\mathrm{cm}^2$ [36], lattice constant $a \approx 4\times10^{-8}$ cm, $\alpha \sim -(0.4\text{–}2)\times10^{-3}$ [13], 0.01–1% concentration of defects provides $n_d = 1.6\times(10^{18}\text{–}10^{20})\,\mathrm{cm}^{-3}$ and so $\rho_s = 7.7\times(10^8\text{–}10^{10})\,Q_{CGSE}\,\mathrm{cm}^{-3}$, $d \cong a/\sqrt[3]{n_d} = (2\text{–}9)\times10^{-7}$cm, $R_D \sim (4\text{–}8)\times10^{-8}$ cm [28], defect radius $r_0 \lesssim a$ and so $\alpha_R + (0.05\text{–}20)\times10^{-2}$. For the aforementioned values of parameters α, R_D and for hypothetical perfect material $D_S \sim (50\text{–}100)\,\mu\mathrm{C\,cm}^{-2} \sim (15\text{–}30)\times10^{-4}\,Q_{CGSE}\,\mathrm{cm}^{-2}$, $\eta \sim (10^{-3}\text{–}10^{-2})$ one obtains that $g \approx (3\times10^{-3}\text{–}2\times10^{-2})/\eta \sim (10^{-2}\text{–}10^{4})\xi \sim -(0.25\text{–}400)$. At $d \sim (5\text{–}10)r_0$ and $\eta \leqslant 0.01$ one obtains $R^2 = \eta(7\text{–}60) \leqslant 1$ (see (A.7) in appendix A). Below we numerically analyse the solution of the system (18) for the following parameters $0 \leqslant R \leqslant 1$, $0.5 < g < 50$, $-1 \leqslant \xi \leqslant -100$.

The equilibrium solution of (18) corresponds to the quasi-static changing external field. For the harmonic modulated applied field $E_m = E_{m0}\sin(w\tau)$ the dimensionless frequency $w = -\alpha\Gamma\omega$ must be much less than unity, we choose $w \sim |, (10^{-4}\text{–}10^{-2})$ and $\Gamma \approx \Gamma_R$. At such low frequencies, the initial conditions determine only the initial curve. They do not play any important role in the loop shape (hereinafter we equate them to zero: $D_m(\tau = 0) = 0$, $\Delta_D^2(\tau = 0) = 0$, $K_{D\rho}(\tau = 0) = 0$).

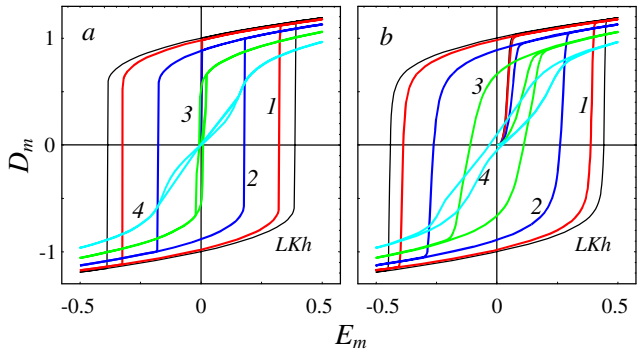

Figure 2. Hysteresis loops at frequencies $w = 2\times10^{-4}$ (a), 2×10^{-2} (b), $R^2 = 0.5$, $\xi = -1$ and for different values of g: 0.1 (curve 1), 0.5 (curve 2), 1 (curve 3), 1.5 (curve 4) and Landau–Khalatnikov loop (curve LKh).

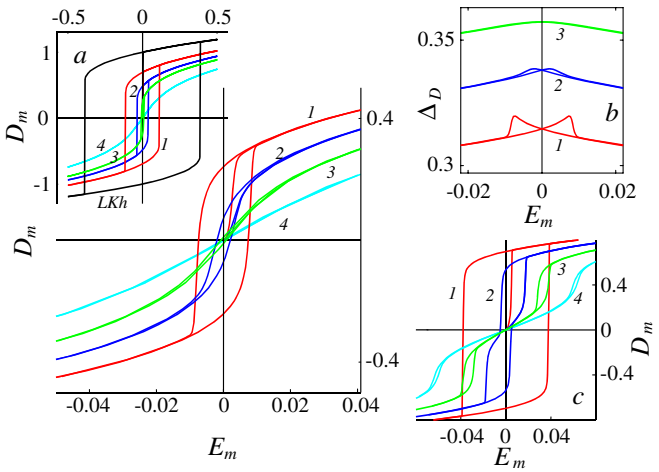

Figure 3. Hysteresis loops for $w = 10^{-4}$, $R^2 = 0.1$ and different values of ξ and g. Basic plot: $D_m(E_m)$; inset b: $\Delta_D(E_m)$: $\xi = -10$, $g = 33$ (curve 1), 35 (curve 2), 37 (curve 3), 40 (curve 4); inset a: $\xi = -10$, $g = 20$ (curve 1), 28 (curve 2), 33 (curve 3), 45 (curve 4) and Landau–Khalatnikov loop (curve LKh); inset c: $\xi = -1$ and $g = 4.5$ (curve 1), 5 (curve 2), 5.5 (curve 3), 6 (curve 4).

The typical hysteresis loops $D_m(E_m)$ obtained at $\xi \sim -1$, $R \sim 0.5$ and different small $g \sim 1$ values are shown in figure 2. Firstly, the increase in g value leads to a decrease in coercive field and then to the appearance of the constriction, subsequent transformation to the double loop and finally to the disappearance of the loop. The broadening, slight tilting and smearing of the loop shape with increase in applied-field frequency can be explained by the increase in dielectric losses. It should be noted that for $R > 1$ and $\xi \to 1$, $g = 0$, $w \to 0$ hysteresis loops are absent [34].

Figure 3 demonstrates the typical changes of hysteresis loop shape caused by increasing the density $\bar{\rho}_s$ (note that $g \sim \bar{\rho}_s$) of charged defects.

At high negative values $\xi \ll -1$ (see inset a), the increase in g value firstly leads to a significant decrease in coercive field and then to the loop disappearance. The coercive fields $E_{cm} \approx 0.0086$ and 0.0024 for the loops 2, 3 in the basic plot are much smaller than the

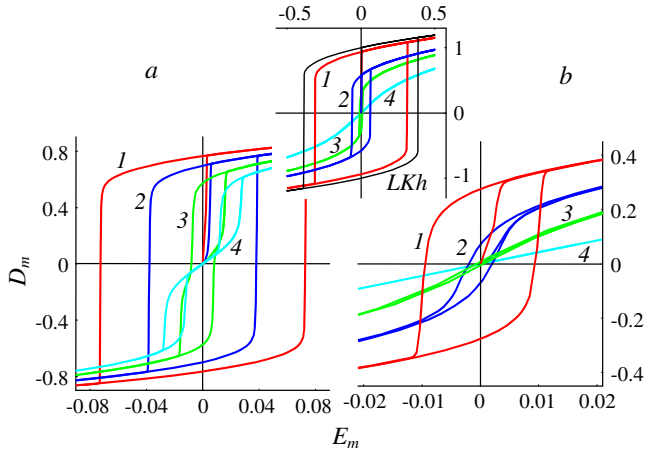

Figure 4. Hysteresis loops, for $w = 10^{-4}$, $g = 5$ and different values of ξ and R^2. (a) $\xi = -1$, $R^2 = 0.08$ (curve 1), 0.09 (curve 2), 0.1 (curve 3), 0.105 (curve 4). (b) $\xi = -10$, $R^2 = 0.65$ (curve 1), 0.7 (curve 2), 0.75 (curve 3), 0.85 (curve 4). Upper inset: $\xi = -10$, $R^2 = 0.1$ (red curve 1), 0.5 (curve 2), 0.65 (curve 3), 1 (curve 4) and Landau–Khalatnikov loop ($R = 0$, curve LKh).

thermodynamic value $E_{cm} \approx 0.39$ for the LKh-loop in inset a. The loop becomes much slimmer rather than lower for increase in charged defect density, $\bar{\rho}_s \sim g$. This effect is somewhat similar to the known 'square-to-slim transition' of the hysteresis loops in some relaxor ferroelectrics [21]. The basic plot demonstrates a drastic decrease in coercive field for $R = 0.1$, $\xi = -10$ and $g > 30$. At small values $|\xi| \leqslant 1$ (see inset c), the increase in g value firstly leads to a decrease in coercive field and then to the constriction appearance, subsequent transformation to the double loop and finally to the loop's disappearance. Inset b demonstrates that the disorder parameter $\Delta_D \neq 0$ over the region of hysteresis. Moreover, it reaches its maximum value near the coercive field, where $\overline{D} \to 0$. This means that the coupled system (17) reveals 'inhomogeneous' displacement switching, e.g. a sample non-polarized as a whole splits into the oppositely polarized regions when the external field reaches a coercive value. In contrast to this, the Landau–Khalatnikov equation describes homogeneous switching with $\delta D \equiv 0$ independently on the external field. Therefore, system (17) is not equivalent to the equations of the Landau–Khalatnikov type.

The typical hysteresis loops obtained at $1 \leqslant g < 10$, for a negative ξ value and different R values are shown in figure 4. At small values $|\xi| \leqslant 1$ (see figure 4(a)), the increase of g value firstly leads to a decrease in coercive field and then to the appearance of the constriction, subsequent transformation to the double loop and finally to the loop's disappearance. At high negative values $\xi \ll -1$ (see figure 4(b)) the loop becomes much slimmer and slightly lower for fluctuations R increasing (compare the Landau–Khalatnikov loop with the other loops). Figure 4(b) demonstrates the drastic decrease of coercive field for $g = 5$ and R^2 values more than 0.6.

Figure 5 demonstrates the typical hysteresis loops at high negative ξ values. A drastic decrease of coercive field corresponds to $\xi \sim -50$ at $g = 35$ and $R^2 = 0.5$. A further increase in ξ value leads to an increase in coercive field. Furthermore, the loop approaches the Landau–Khalatnikov curve at $\xi \to -\infty$.

One can notice from figures 3–5 that the following scaling exists at $\xi \ll -1$: the calculated hysteresis loops reveal a drastic decrease in coercive field value at $-gR^2/\xi \geqslant 0.3$. In appendix C we obtain the estimations for static remanent displacement $D_r \equiv \overline{D}(\omega = 0, E_0 = 0)$, linear

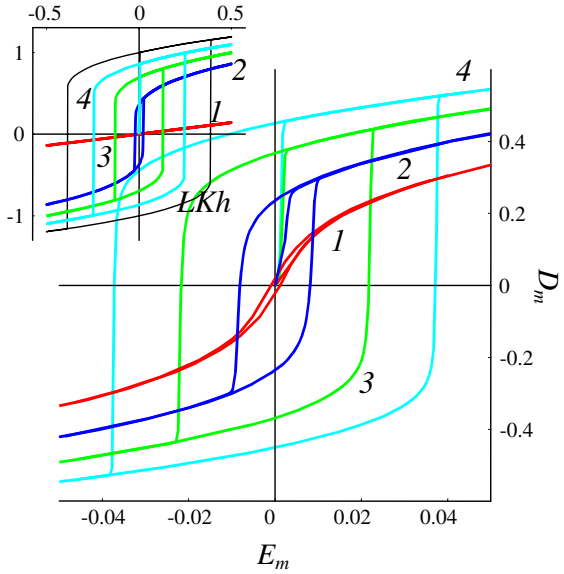

Figure 5. Hysteresis loops for $w = 10^{-4}$; $g = 35$, $R^2 = 0.5$ and different values of ξ : -50 (curve 1), -55 (curve 2), -60 (curve 3), -65 (curve 4). Inset: $\xi = -10$ (curve 1), -50 (curve 2), -100 (curve 3), -200 (curve 4) and Landau–Khalatnikov loop (curve LKh).

dielectric permittivity $\varepsilon_r \equiv \mathrm{d}\overline{D}(\omega = 0, E_0 = 0)/\mathrm{d}E_0$ and coercive field value $E_C(\omega = 0)$, namely at $|\xi| \gg 1$:

$$D_r \sim D_S\sqrt{1+\frac{3gR^2}{\xi}}, \qquad \varepsilon_r \sim \frac{1}{-2\alpha(1+3gR^2/\xi)}, \qquad |E_C| \sim \frac{2|\alpha D_S|}{3\sqrt{3}}\left(1+\frac{3gR^2}{\xi}\right)^{3/2}. \tag{19}$$

Note that the set of equations (19) is valid for $R < 1$, $\xi > -10$, $g > 5$ with 10% accuracy. Really, at $\xi \ll -1$, D_r, ε_r and E_C depend on the combination $-gR^2/\xi \approx 16\pi^2 d^2 \delta\rho_s^2/D_s^2$, with the transition point at $-gR^2/\xi \sim 0.3$.

We can conclude that the increasing of charged defect concentration (as well as its fluctuations) leads to a drastic decrease in the coercive field, appearance of constricted and double hysteresis loops related to the inhomogeneous displacement switching. We demonstrate that this result agrees much better with experiments in thick films and bulk samples, than predictions of conventional Landau–Ginzburg and nucleation theories as shown in the next section.

6. Comparison with experiment

Solid solutions $Pb(Zr,Ti)O_3$ (PZT) are widely used ferroelectrics, however much more work is needed to determine the physics of these materials [13]. A wide range of low-level additives (0.0–5.0%) significantly influence the dielectric properties of PZT at room temperature. At liquid-helium temperatures, all these 'extrinsic' effects disappear and the experimental data agree with 'single domain' intrinsic permittivity calculated from thermodynamic theory. At room temperature, donor additives such as La, Nb, Nd or Ce 'soften' PZT dielectric properties;

Table 1. Data for 'soft' $Pb(Zr_xTi_{1-x})O_3$ films.

Composition, Ref., method	Substrate, doping	Top electrode	Thickness (μm)	$\varepsilon_r(E=0)$ calc. from the loop	Ampl. E_0 (kV cm^{-1})	Rem. displacement D_r (μC cm^{-2})	Coercive field E_C (kV cm^{-1})
$x = 0.52$,	$SrRuO_3$/Si,	Ag, Au	1.4	2800	400	28	+96, −70
PZT-LQ [19],	Nb-modified		20	3500	400	±28	±52
$\omega \sim 100$ Hz,							
$T = 25$°C, ADM			Our fitting (figure 6)	2700	400	±25	±52
$x = 0.54$, [20],	Pt/Si, 1% Nb	Pt	1.9	∼3000	105	+25	−23
$\omega \sim 1$ kHz,						−28	+33.5
$T = 25$°C, RFMS			Our fitting (figure 8)	∼4000	105	+20	−22.5
						−25	+32.5

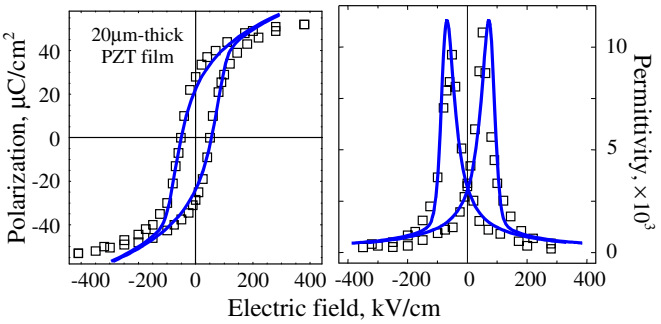

Figure 6. Hysteresis loop observed in a 20 μm thick Nb-modified PZT film fabricated by aerosol deposition method (ADM). Squares are experimental data from [19] at $E_0 = 400\,\mathrm{kV\,cm^{-1}}$, solid curve is our fitting at $w = 0.017$, $\xi \leqslant -10$, $gR^2/\xi = -0.34$ (scaling region) and $D_S = 72\,\mu\mathrm{C\,cm^{-2}}$, $E_S = 269\,\mathrm{kV\,cm^{-2}}$ calculated from [13] at $x = 0.5$.

in particular, hysteresis loops have a rather high remanent displacement and low coercive field [13]. We suppose that aforementioned dopants as well as numerous unavoidable Pb vacancies (originating due to the high volatility of PbO, see chapter 10 in [12]) play the role of randomly distributed charged defects.

For thick $Pb(Zr_xTi_{1-x})O_3$ films ($x \sim 0.5$, $\ell \geqslant 2\,\mu$m) and bulk samples, typical values are the following: remanent displacement $D_r = (20\text{–}50)\,\mu\mathrm{C\,cm^{-2}}$ and coercive field $E_C = (10\text{–}100)\,\mathrm{kV\,cm^{-1}}$ (see [13] and table 1). Usually, the ferroelectric hysteresis loops of 'soft' PZT films, obtained with the help of the conventional Sawyer–Tower circuit at low frequency ($\omega \sim (0.1\text{–}1)$ kHz), are rather 'thin' and 'sloped' (see figures 6 and 8).

For PZT Landau–Ginsburg free energy expansion coefficients $\alpha(x)$, $\beta(x)$ strongly depends on the Zr molar fraction x. Near the morphotropic boundary $x \approx 0.5$, PZT is ferroelectric with the second-order phase transition ($\beta > 0$).

For the Landau–Ginsburg free energy expansion $\alpha D^2/2 + \beta D^4/4 + \chi D^6/6 + \cdots$, the following data are known: $\alpha(0.50\text{–}0.54) = -(9.8\text{–}12.2) \times 10^7\,\mathrm{m\,F^{-1}}$, $\beta(0.50\text{–}0.54) = (19.1\text{–}33.2) \times 10^7\,\mathrm{m^5\,C^{-2}\,F^{-1}}$ (obtained by linear interpolation of data from table 7.1 in [13] at $T = 25\,^\circ$C, SI units). From these data it is easy to calculate the Landau–Ginsburg remanent displacement $D_r = \sqrt{-\alpha/\beta} \approx (72\text{–}61)\,\mu\mathrm{C\,cm^{-2}}$ and static ($\omega = 0$) thermodynamic coercive field $E_C = 2\sqrt{-\alpha^3/27\beta} \approx (269\text{–}284)\,\mathrm{kV\,cm^{-1}}$ in D^4-approximation. These values do not

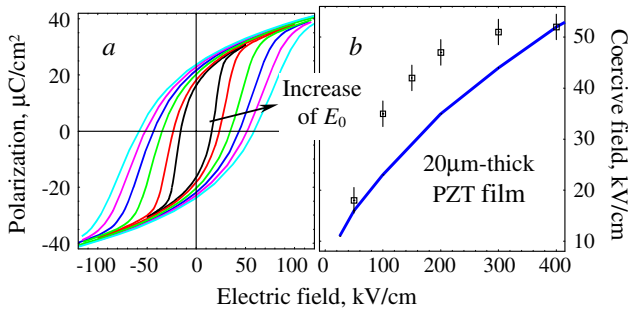

Figure 7. Hysteresis loop shape at different electric field amplitudes E_0: 50, 100, 200, 300, 400 and 500 kV cm^{-1} (a). Coercive field as a function of applied electric field amplitude (b). □, experimental data for 20 μm thick Nb-modified PZT film [19]; —, our theory. Parameters are the same as in figure 6.

match experimental data for D_r and E_C (see table 1). In order to improve the calculations for D_r, a higher coefficient $\chi(0.5\text{–}0.54) = (8.0\text{–}11.3) \times 10^8$ m^7 C^4 F^{-1} is used [13], but even such an approach leads to the significantly overestimated values of $E_C \geqslant 250$ kV cm^{-1}.

The observed values of D_r and E_C depend not only on the composition x, but on the film thickness, fabrication method, substrate material, etc. The thickness-driven correlation effects [14] should be neglected if only the film thickness $\ell \gg \gamma/\lambda|\alpha|$. For the typical values of surface extrapolation length $\lambda \leqslant 10^{-8}$ m, the gradient term $\gamma \leqslant 10^{-7}$ F · m and $|\alpha| \sim 10^{+8}$ m F^{-1} far from Curie temperature [1], one obtains that thickness-driven effects become noticeable only for $\ell \leqslant 0.5\,\mu$m. So, for μm-thick PZT films we can neglect thickness-driven effects and use the results (17)–(19). However, up to 5 μm films such interface phenomena as film–substrate mismatch and charged layers cause asymmetry in loops [15] due to the induced electric field, and mismatch-induced homogeneous elastic stresses renormalize the free-energy coefficients α and β [37].

In accordance with (18) and (19) we regard values $D_S = \sqrt{-\alpha/\beta}$, $E_S = 2\alpha D_S/3\sqrt{3}$ as hypothetical ones for perfect PZT at morphotropic boundary $x = 0.5$, values $w \ll -1$ and gR^2/ξ ($\xi \ll -1$) as fitting parameters determined by unavoidable cation vacancies depending on molar fraction x and/or Nb^{5+} concentration. Our fitting is presented in figures 6–8. The discrepancy at high external field between the calculated and measured values is considered to be due to the D^4-approximation used in our model. In order to improve the fitting, the higher-order terms D^6, ... should be taken into account.

The nucleation theory gives the coercive field value independent of the external field amplitude E_0. At low frequencies ($w \leqslant 0.1$), the Landau–Khalatnikov equation gives coercive field values very close to the thermodynamic limit $2\sqrt{-\alpha^2/27\beta}$ almost independent of the external field amplitude E_0 (the so-called saturated 'square' loops), whereas experiment data for PZT show its strong dependence on E_0 (see figure 7(b)). In contrast to the Landau–Khalatnikov model, our model shows quantitative agreement with experiment (see figure 7).

The right-hand side shift of the 1.9 μm thick PZT film is related to the lacking layer near the boundary metal–semiconductor at the bottom electrode (see chapter 14 in [38] and figure 8).

It follows from table 1 and figures 6–8 that our model can quantitatively describe typical ferroelectric hysteresis loops in thick 'soft' PZT films. In particular, it gives correct coercive field values and its dependence on external-field amplitude.

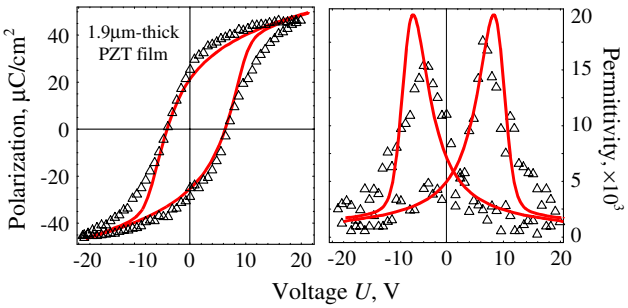

Figure 8. Centred hysteresis loop observed in a 1.9 μm thick 'soft' PZT film manufactured by RF magnetron sputtering (RFMS). △, experimental data given by authors of [20]; —, our fitting at $w = 0.02$, $gR^2/\xi = -0.36$ ($\xi = -4$, $R = 1$, $g = 1.45$) and $D_S = 72\,\mu\mathrm{C\,cm^{-2}}$, $E_S = 269\,\mathrm{kV\,cm^{-1}}$ ($U_S = 51.2\,\mathrm{V}$).

The constricted and double loops were observed in PZT ceramics doped with Nd [18] and La [24, 25]. Sometimes constricted loops disappear after baking at high pressures, annealing in special atmospheres or after several hundreds of switching cycles [18, 24, 25]. In order to explain this effect, we assume that ceramics treatment or fatigue can cause a significant change in the spatial distribution of charged defects (e.g. the characteristic distance d and concentration n_d). The latter leads to the changing of gR^2 and ξ values in accordance with (18). Thus either appearance of constricted and double hysteresis loops in aged materials [18, 25] or their disappearance depends on the values of the parameters R, ξ and g after sample treatment.

It should be noted that the origin of the constricted or double loops in aged ferroelectric $BaTiO_3$ and (Pb,Ca)TiO_3 ceramics is caused by the mechanical clamping of spontaneous polarization switching [12] and so it lies outside our theoretical consideration. This may be related to the fact that possible evolution of the charge fluctuations caused by the relaxation/origin of internal stresses around defects was not taken into account in our model.

Let us briefly compare our theoretical results with classical ones concerning lightly donor-doped $BaTiO_3$. In many cases, the presence of non-isovalent additives or unavoidable impurities, even in very restricted quantity, significantly attenuates piezoelectric properties of $BaTiO_3$ ceramics, increases electrical conductivity, diffuses the peak of dielectric response and makes the hysteresis loop slim for low coercive field (see chapter 5 in [12]). Therefore, we consider the influence of charged defects on the ferroelectric properties of such 'soft' materials, neglecting the contribution of inhomogeneous mechanical deformations arising due to intergranular stresses as well as local symmetry distortion appearing near the defects.

The 0.1–0.3% of La, Nb or Ce-doping changes a wide band-gap intrinsic semiconductor $BaTiO_3$ to an extrinsic n-type semiconductor, achieved by replacing Ba^{2+} or Ti^{4+} with ions Le^{3+}, Ce^{3+} or Nb^{5+} with higher valency [12, 39]. In most of the $BaTiO_3$ ceramics, unavoidable impurities such as Fe^{3+} are present. In such a case, the sample has a slightly brown hue. Such ceramics reveal 'soft' hysteresis loops with small area and low coercive field, diffuse dielectric properties and disappearance of spontaneous displacement (see [12], table 2), in contrast to $BaTiO_3$ single crystals which undergo a first-order phase transition with abrupt disappearance of displacement at $T = 110\,^{\circ}\mathrm{C}$. We suppose that coupled equations (18) evolved for ferroelectrics with second-order phase transition can be applied to the doped or 'soft' $BaTiO_3$ ceramics. Obtained results are summarized in figure 9 and table 2.

Table 2. Data for $BaTiO_3$ ceramics.

Composition, doping of bulk $BaTiO_3$ ceramics	Experimental values figures 5.16 and 5.33 in [12], $T = 25\,^{\circ}C$, $\omega = 60\,Hz$, $E_0 = 15\,kV\,cm^{-1}$		Landau–Ginsburg theory for pure bulk $BaTiO_3$, $T = 25\,^{\circ}C$ $\ell \to \infty$		Nucleation theory [6] $E_C \sim (\frac{1}{\ell})^{2/9}$	Our fitting at $\ell \to \infty$ (see figure 9)	
	E_C ($kV\,cm^{-1}$)	D_r ($\mu C\,cm^{-2}$)	E_C ($kV\,cm^{-1}$)	D_r ($\mu C\,cm^{-2}$)	E_C ($kV\,cm^{-1}$)	E_C ($kV\,cm^{-1}$)	D_r ($\mu C\,cm^{-2}$)
Soft	3.5	7.5	200	25	1 ($\ell = 25\,\mu m$)	4	7.5
3% Nb	0.94	0.8			0 ($\ell \to \infty$)	1	0.8

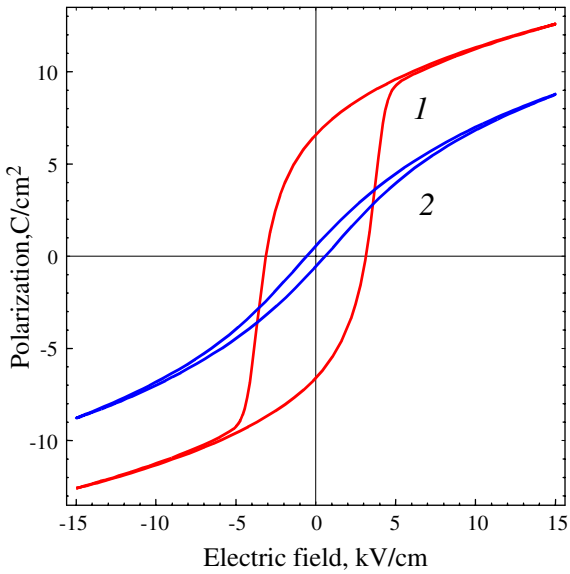

Figure 9. Our fitting for hysteresis loop observed in $BaTiO_3$ ceramics (see figures 5.16 and 5.33 in [12]) obtained at $E_0 = 15\,kV\,cm^{-1}$, $\xi \leqslant -10$, $w = 0.005$, $E_S = 200\,kV\,cm^{-1}$, $D_S = 25\,\mu C\,cm^{-2}$. Curve 1, 'soft' ceramics ($gR^2\,\xi = -0.33$); curve 2, ceramics doped with 3% of Nb ($gR^2\,\xi = -0.39$).

It follows from table 2 and figure 9 that our model can quantitatively describe typical ferroelectric hysteresis loops in 'soft' $BaTiO_3$ ceramics; in particular, it gives correct coercive field values.

7. Conclusion

We have proposed a phenomenological description of polarization switching peculiarities in ferroelectric semiconductors with charged defects and prevailing extrinsic conductivity. Specifically, we modified the Landau–Ginsburg approach for the aforementioned inhomogeneous systems and obtained the system of coupled equations (17). Solving the system (17) one can get information about system ordering as a whole, without defining space distribution of the appeared displacement inhomogeneities; however the present model

has the following advances over the conventional ones and our previously published works [15, 34, 35]:

- The coupled system (17) reveals inhomogeneous displacement switching in contrast to the Landau–Khalatnikov equation, which describes the homogeneous one.
- We have shown that increasing the charged defect concentration (as well as its fluctuations) leads to a drastic decrease of the coercive field and the appearance of constricted and double hysteresis loops.
- The obtained results quantitatively describe typical ferroelectric hysteresis loops in thick donor-doped PZT films and $BaTiO_3$ ceramics; in particular, our model gives correct coercive field values and its dependence over external field amplitude, in contrast to the conventional Landau–Ginsburg and nucleation theories.

Acknowledgments

The author is greatly indebted to Professor N V Morozovsky for fruitful discussions of the model and useful remarks and Professor D Remiens for providing experimental data. This work is supported by grant INTAS-01-0173.

Appendix A

Let us estimate the dependence of parameters η and R^2 on the distribution characteristics of charged defects. Values of the average distance d between them and size r_0 can be expressed via defect concentration n_d and lattice constant a as $d = a/\sqrt[3]{n_d}$, $r_0 \sim a$. If charged defects are clustered, the distance d can be several times greater than $1/\sqrt[3]{n_d}$. We consider the case when defects' concentration n_d is not more than a few per cent, i.e. $d > 3r_0$ (see figure 1). For the sake of simplicity, we approximate the defects' charge densities by isotropic Gaussian distributions:

$$\rho_s(\mathbf{r}) = \sum_{i=1}^{N} \frac{q_i}{\pi^{3/2} r_{0i}^3} \exp\left[-\frac{(\mathbf{r} - \mathbf{r}_i)^2}{r_{0i}^2} \right]. \tag{A.1a}$$

The charge density of screening clouds of carriers that originated around charge defects can be estimated in Gaussian approximation using the Debye potential [40] and the Green's function method, namely at $r_0 \sim R_D$ we obtain:

$$n(\mathbf{r}) \approx n_f + \sum_{i=1}^{N} \frac{e_i}{\pi^{3/2}(r_{0i} + R_D)^3} \exp\left[-\frac{(\mathbf{r} - \mathbf{r}_i)^2}{(r_{0i} + R_D)^2} \right]. \tag{A.1b}$$

Here n_f is the charge density of free electrons in the conduction band of an extrinsic semiconductor [28, 38]. In our case, a high-defect concentration, $n_d \sim 1\,\%$, provides $n_f \approx \bar{n} = -\bar{\rho}_s$, and so only the relatively small amount of electron charge e_i is localized near charged defects q_i.

In the hypothetical case, when all impurity atoms are identical and regularly distributed, one obtains that $q_i \equiv q_0, e_i \equiv e_0, r_{0i} \equiv r_0, |\mathbf{r}_{i+1} - \mathbf{r}_i| \equiv d$ and thus we obtain from (A.1) that

$$\bar{\rho}_s = \frac{N}{V} \int_V \mathrm{d}^3\mathbf{r} \, \frac{q_0}{\pi^{3/2} r_0^3} \exp\left(-\frac{r^2}{r_0^2} \right) = q_0 \frac{N}{V} \equiv \frac{q_0}{d^3}, \tag{A.2}$$

$$\bar{n} = n_f + \frac{N}{V} \int_V \mathrm{d}^3\mathbf{r} \, \frac{e_0}{\pi^{3/2}(r_0 + R_D)^3} \exp\left(-\frac{r^2}{(r_0 + R_D)^2} \right) = n_f + \frac{e_0}{d^3}. \tag{A.3}$$

It is obvious from (A.2) and (A.3) that $q_0 = \bar{\rho}_s d^3$ and $e_0 = -(\bar{\rho}_s + n_f)d^3$ leading to $-\bar{\rho}_s = \bar{n}$. Similarly to (A.2) and (A.3) we calculate that

$$\overline{\rho_s(\mathbf{r})n(\mathbf{r})} = \bar{\rho}_s n_f - \frac{\bar{\rho}_s(n_f + \bar{\rho}_s)}{[1 + r_0^2/(r_0 + R_D)^2]^{3/2}} \left(\frac{d}{\sqrt{\pi} r_0}\right)^3, \qquad \overline{\rho_s^2(\mathbf{r})} = \bar{\rho}_s^2 \left(\frac{d}{\sqrt{2\pi} r_0}\right)^3. \tag{A.4}$$

Now it is easy to find the correlations

$$\overline{\delta\rho_s\, \delta n} \equiv \overline{(\rho_s - \bar{\rho}_s)(n - \bar{n})} = \overline{\rho_s n} + \bar{\rho}_s^2, \qquad \overline{\delta\rho_s^2} \equiv \overline{(\rho_s - \bar{\rho}_s)^2} = \overline{\rho_s^2} - \bar{\rho}_s^2. \tag{A.5}$$

With the help of the above-mentioned assumptions and calculations (A.2)–(A.5) it is easy to obtain that

$$\overline{\delta\rho_s\, \delta n} = \bar{\rho}_s(n_f + \bar{\rho}_s) \left(\frac{(d/\sqrt{\pi} r_0)^3}{[1 + r_0^2/(r_0 + R_D)^2]^{3/2}} - 1\right), \qquad \overline{\delta\rho_s^2} = \bar{\rho}_s^2 \left(\left(\frac{d}{\sqrt{2\pi} r_0}\right)^3 - 1\right). \tag{A.6}$$

Using the definitions $R^2 = -\overline{\delta\rho_s\, \delta n}/\bar{\rho}_s^2 \equiv \eta\overline{\delta\rho_s^2}/\bar{\rho}_s^2$ and $\eta \approx -\overline{\delta\rho_s\, \delta n}/\overline{\delta\rho_s^2}$, one derives from (A.6):

$$R^2 = \left(1 + \frac{n_f}{\bar{\rho}_s}\right) \left(\frac{(d/\sqrt{\pi} r_0)^3}{[1 + r_0^2/(r_0 + R_D)^2]^{3/2}} - 1\right),$$

$$\eta \leqslant \left(1 + \frac{n_f}{\bar{\rho}_s}\right) \left(\frac{2}{(1 + R_D/r_0)^2 + 1}\right)^{3/2}. \tag{A.7}$$

Allowing for $n_f \approx -\bar{\rho}_s$, we obtain that always $\eta \ll 1$. Thus at $d \sim$ (5–10)r_0 and $\eta \leqslant 0.01$, $R^2 = \eta$(7–60) $\leqslant 1$. However, when defects' concentration becomes very small, e.g. for $d \to \infty$ and $n_d \to 0$, intrinsic conductivity could not be neglected in comparison with the extrinsic case and therefore the obtained expressions (A.6) and (A.7) become incorrect.

Appendix B

The equations for $\overline{\delta D^2}$ and $\overline{\delta D\, \delta\rho_s}$ obtained directly from (12) have the form:

$$\frac{\Gamma}{2}\frac{\partial}{\partial t}\overline{\delta D^2} + (\alpha + 3\beta\overline{D}^2(t))\,\overline{\delta D^2} + \beta\,\overline{\delta D^4} = \gamma\,\overline{\delta D \frac{\partial^2\, \delta D}{\partial \mathbf{r}^2}} + \overline{\delta D\, \delta E_z}, \tag{B.1}$$

$$\Gamma\frac{\partial}{\partial t}\,\overline{\delta D\, \delta\rho_s} + (\alpha + 3\beta\overline{D}^2(t))\,\overline{\delta D\, \delta\rho_s} + \beta\,\overline{\delta D^3 \delta\rho_s} = \gamma\,\overline{\delta\rho_s \frac{\partial^2\, \delta D}{\partial \mathbf{r}^2}} + \overline{\delta\rho_s\, \delta E_z}. \tag{B.2}$$

On multiplying (12) by δD^2 or $\delta\rho_s\, \delta D$ and averaging, using (5) and (6), one obtains that

$$\overline{\delta D^4} = (\overline{\delta D^2})^2, \qquad \overline{\delta D^3\, \delta\rho_s} = \overline{\delta D^2}\,\overline{\delta D\, \delta\rho_s}. \tag{B.3}$$

Taking into account that the average period of the distribution of inhomogeneities is d (see figure 1), one obtains that $\partial/\partial\mathbf{r} \sim \mathrm{i}/d$ and so

$$\gamma\,\overline{\delta D \frac{\partial^2\, \delta D}{\partial \mathbf{r}^2}} \sim -\frac{\gamma}{d^2}\,\overline{\delta D^2}, \qquad \gamma\,\overline{\delta\rho_s \frac{\partial^2\, \delta D}{\partial \mathbf{r}^2}} \sim -\frac{\gamma}{d^2}\,\overline{\delta\rho_s\, \delta D}. \tag{B.4}$$

Let us express the field variation δE_z using δD and $\delta\rho_s$. In accordance with (17),

$$\delta E_z \approx \frac{\partial}{\partial t}\frac{\delta D}{4\pi\mu\bar{\rho}_s} - E_0(t)\left(\frac{\delta\rho_s}{\bar{\rho}_s} - \frac{\mathrm{div}(\delta\mathbf{D})}{4\pi\bar{\rho}_s}\right) + \frac{\kappa}{\mu}\frac{\partial}{\partial z}\frac{\delta\rho_s}{\bar{\rho}_s} - \frac{\kappa}{\mu}\frac{\partial}{\partial z}\frac{\mathrm{div}(\delta\mathbf{D})}{4\pi\bar{\rho}_s} + \frac{\delta n\, \delta E_z - \overline{\delta n\, \delta E_z}}{\bar{\rho}_s}. \tag{B.5}$$

For a thick sample with equivalent boundaries $z = \pm\ell$ the term

$$\overline{\frac{\partial}{\partial z}\delta D^2}$$

is equal to zero. In accordance with comments to (6) $\overline{\delta n\,\delta E_z^2} = 0$ and $\overline{\delta\rho_s\,\delta n\,\delta E_z} = 0$; thus one can derive from (B.5) the following approximations for the correlations:

$$\overline{\delta D\,\delta E}_z = \frac{1}{8\pi\mu\bar{\rho}_s}\frac{\partial}{\partial t}\overline{\delta D^2} - E_0(t)\frac{\overline{(\delta\rho_s\,\delta D)}}{\bar{\rho}_s} + \frac{\kappa}{\mu}\overline{\left(\delta D\frac{\partial}{\partial z}\frac{\delta\rho_s}{\bar{\rho}_s}\right)} - \frac{\kappa}{4\pi\bar{\rho}_s\mu}\overline{\delta D\frac{\partial}{\partial z}\operatorname{div}(\delta\mathbf{D})}. \tag{B.6}$$

In accordance with (13) the term

$$\frac{\kappa}{\mu}\overline{\left(\delta D\frac{\partial}{\partial z}\frac{\delta\rho_s}{\bar{\rho}_s}\right)} = -\frac{\kappa}{\mu\bar{\rho}_s}\overline{\left(\delta\rho_s\frac{\partial}{\partial z}\delta D\right)}$$

can be estimated as

$$-\frac{4\pi\kappa}{\mu\bar{\rho}_s}\overline{\delta\rho_s(\delta\rho_s+\delta n)} \approx -(1-\eta)\frac{4\pi\kappa}{\mu\bar{\rho}_s}\overline{\delta\rho_s^2}.$$

In accordance with the definition of Debye radius $R_D = \sqrt{\kappa/4\pi n\mu}$, this term $-(1-\eta)(4\pi\kappa/\mu\bar{\rho}_s)\,\overline{\delta\rho_s^2} = 16\pi^2R_D^2(1-\eta)\,\overline{\delta\rho_s^2}$. Taking into account that the average period of the distribution of inhomogeneities is d (see figure 1), the last term in the right-hand side of (B.6) can be estimated as

$$\frac{\kappa}{4\pi\bar{\rho}_s\mu}\overline{\frac{\partial\,\delta D}{\partial z}\operatorname{div}(\delta\mathbf{D})} \sim \frac{\kappa}{4\pi\bar{\rho}_s\mu}\overline{\left(\frac{\partial\,\delta D}{\partial z}\right)^2} = -\frac{R_D^2}{d^2}\,\overline{\delta D^2}.$$

Thus the correlation

$$\overline{\delta D\,\delta E}_z = \frac{1}{8\pi\mu\bar{\rho}_s}\frac{\partial}{\partial t}\overline{\delta D^2} - E_0(t)\frac{\overline{(\delta\rho_s\,\delta D)}}{\bar{\rho}_s} + 16\pi^2R_D^2(1-\eta)\,\overline{\delta\rho_s^2} - \frac{R_D^2}{d^2}\,\overline{\delta D^2}. \tag{B.7}$$

For a thick sample with equivalent boundaries $z = \pm\ell$, the term $\overline{\partial(\delta\rho_s^2/\bar{\rho}_s)/\partial z}$ is equal to zero and therefore we obtain from (B.5) that

$$\overline{\delta\rho_s\,\delta E}_z = \frac{1}{4\pi\mu\bar{\rho}_s}\frac{\partial}{\partial t}\overline{\delta\rho_s\,\delta D} + E_0(t)\frac{\overline{\delta\rho_s\delta n}}{\bar{\rho}_s} - \frac{\kappa}{4\pi\bar{\rho}_s\mu}\overline{\delta\rho_s\frac{\partial}{\partial z}\operatorname{div}(\delta\mathbf{D})}. \tag{B.8}$$

In accordance with (13) the last two terms on the right-hand side of (B.6) can be estimated as

$$E_0(t)\frac{\overline{\delta\rho_s\,\delta n}}{\bar{\rho}_s} \approx -\eta\frac{\overline{\delta\rho_s^2}}{\bar{\rho}_s}E_0(t), \qquad \frac{\kappa}{4\pi\bar{\rho}_s\mu}\overline{\delta\rho_s\frac{\partial}{\partial z}\operatorname{div}(\delta\mathbf{D})} \sim -\frac{\kappa}{4\pi\bar{\rho}_s\mu d^2}\,\overline{\delta\rho_s\,\delta D} = \frac{R_D^2}{d^2}\,\overline{\delta\rho_s\,\delta D}$$

and so

$$\overline{\delta\rho_s\,\delta E}_z = \frac{1}{4\pi\mu\bar{\rho}_s}\frac{\partial}{\partial t}\overline{\delta\rho_s\,\delta D} - \eta\frac{\overline{\delta\rho_s^2}}{\bar{\rho}_s}E_0(t) - \frac{R_D^2}{d^2}\,\overline{\delta\rho_s\,\delta D}. \tag{B.9}$$

Thus gradient terms in (B.1) and (B.2) can be either neglected at $(\gamma + R_D^2)/d^2 \ll \alpha$ or the coefficient α can be renormalized as $\alpha \to \alpha_R = (\alpha + (\gamma + R_D^2)/d^2)$. Using (B.3), (B.4), (B.7) and (B.9) we obtain the equations (18b) and (18c) from the equations (B.1) and (B.2).

Appendix C

In the stationary case ($\omega \to 0$, $\partial/\partial t \equiv 0$), the correlation $\overline{\delta D\, \delta\rho_s}$ can be expressed via $\overline{D}^2$ and $\overline{\delta D^2}$ from (17.c); thus the equation (17.b) acquires the form:

$$\overline{\delta D^2} = \frac{E_0^2 R^2}{(\alpha_R + 3\beta\overline{D^2} + \beta\overline{\delta D^2})^2} + \frac{\vartheta}{(\alpha_R + 3\beta\overline{D^2} + \beta\,\overline{\delta D^2})}. \tag{C.1}$$

As it follows from equation (17.a), $\overline{\delta D^2} = (E_0 - \alpha\overline{D} - \beta\overline{D}^3)/3\beta\overline{D}$, and the modified equation for $\overline{D}$ can be obtained directly from (C.1), namely

$$\left[\alpha + \frac{3\beta(E_0^2R^2 + \vartheta(\alpha_R - \alpha/3 + 8\beta\overline{D}^2/3 + E_0/3\overline{D}))}{(\alpha_R - \alpha/3 + 8\beta\overline{D^2}/3 + E_0/3\overline{D})^2}\right]\overline{D} + \beta\overline{D}^3 = E_0. \tag{C.2}$$

Let us recall that $\vartheta = (4\pi R_D)^2(1-\eta)\,\overline{\delta\rho_s^2}$, $D_S^2 = -\alpha/\beta$, $R^2 = \eta\,\overline{\delta\rho_s^2}/\bar{\rho}_s^2$ (see (18)).

(1) The remanent (spontaneous) displacement $D_r \equiv \overline{D}(E_0 = 0)$ obtained from (C.2) satisfies the following biquadratic equation:

$$D_r^2 = D_S^2\left[1 - \frac{3\vartheta/D_S^2}{(\alpha_R - \alpha/3 + 8\beta D_r^2/3)}\right]. \tag{C.3}$$

As should be expected, the value $D_r^2 = D_S^2$ obtained in the Landau–Ginzburg model is the zero approximation in (C.3) over the parameter $\vartheta/(\alpha D_S^2)$. Thus, in the first approximation over parameter $\vartheta/(\alpha D_S^2)$, one derives from (C.3) that

$$D_r^2 \approx D_S^2\left[1 - \frac{3\vartheta/D_S^2}{\alpha_R - 3\alpha}\right]. \tag{C.4}$$

(2) The static linear dielectric permittivity $\varepsilon_r \equiv \mathrm{d}\overline{D}(E_0 = 0)/\mathrm{d}E_0$ obtained from (C.2) satisfies the following linear equation:

$$\varepsilon_r\left[\alpha + \frac{3\beta\vartheta}{(\alpha_R - \alpha/3 + 8\beta D_r^2/3)} - \frac{16\beta^2\vartheta D_r^2}{(\alpha_R - \alpha/3 + 8\beta D_r^2/3)^2} + 3\beta D_r^2\right] = 1 + \frac{\beta\vartheta}{(\alpha_R - \alpha/3 + 8\beta D_r^2/3)^2}.$$

In accordance with (C.3)

$$\alpha + \frac{3\beta\vartheta}{(\alpha_R - \alpha/3 + 8\beta D_r^2/3)} = -\beta D_r^2,$$

and thus we obtain

$$\varepsilon_r = \left[1 + \frac{\beta\vartheta}{(\alpha_R - \alpha/3 + 8\beta D_r^2/3)^2}\right]\left[2\beta D_r^2 - \frac{16\beta^2\vartheta D_r^2}{(\alpha_R - \alpha/3 + 8\beta D_r^2/3)^2}\right]^{-1}. \tag{C.5}$$

As should be expected, the value $\varepsilon_R \equiv 1/(-2\alpha)$ obtained in the Landau–Ginzburg model is the zero approximation in (C.5) over the parameter $\vartheta/(\alpha D_S^2)$. Thus, in the first approximation over the parameter $\vartheta/(\alpha D_S^2)$ one derives from (C.4) and (C.5) that

$$\varepsilon_r \approx \frac{1}{-2\alpha}\left[1 + \frac{3\beta\vartheta}{(\alpha_R - 3\alpha)\alpha} - \frac{9\beta\vartheta}{(\alpha_R - 3\alpha)^2}\right]^{-1}. \tag{C.6}$$

(3) The static coercive field value $E_C(\overline{D} = 0)$ can be determined from the divergence of generalized permittivity, namely from the condition $\mathrm{d}\overline{D}(E_0 = E_C)/\mathrm{d}E_0 \to \infty$. Thus,

the condition of zero denominator in the cumbersome expression for $\mathrm{d}\overline{D}(E_0)/\mathrm{d}E_0$ obtained directly from (C.2), gives the following equation for coercive field value determination:

$$E_C = -2\beta\overline{D}^3 + \frac{\beta(16\beta\overline{D}^3 - E_C)(2E_C^2R^2 + \vartheta(\alpha_R - \alpha/3 + 8\beta\overline{D}^2/3 + E_C/3\overline{D}))}{(\alpha_R - \alpha/3 + 8\beta\overline{D}^2/3 + E_C/3\overline{D})^3}. \tag{C.7}$$

Equation (C.7) is solved coupled with (C.2) at $E_0 = E_C$, and the couple of values $\{\overline{D}(E_C), E_C\}$ can be found at least numerically. As should be expected, the values $\{\overline{D} = D_S/\sqrt{3},\quad E_C = -2\beta\overline{D}^3 \equiv 2\alpha D_S/3\sqrt{3}\}$ obtained in the Landau–Ginzburg model are the zero approximation in (C.7) and (C.2) over the parameters R and $\vartheta/(\alpha D_S^2)$. Thus, in the first approximation over these parameters, one derives from (C.2) and (C.7) the following system:

$$E_C \approx \begin{cases} \alpha\overline{D}(E_C)[1+\nu_1] + \beta\overline{D}^3(E_C), \\ -2\beta\overline{D}^3(E_C)[1+\nu_2], \end{cases} \tag{C.8a}$$

$$\nu_1 = -\frac{4\alpha^2R^2}{9(\alpha_R-\alpha)^2} + \frac{3\beta\vartheta}{(\alpha_R-\alpha)\alpha}, \qquad \nu_2 = \frac{8\alpha^3R^2}{3(\alpha_R-\alpha)^3} - \frac{9\beta\vartheta}{(\alpha_R-\alpha)^2}. \tag{C.8b}$$

In the first approximation over parameters $\nu_{1,2}$, one derives from the system (C.8) that

$$E_C = \frac{2\alpha D_S}{3\sqrt{3}}\left(1 + \frac{3\nu_1}{2}\right), \qquad \overline{D}(E_C) = \frac{D_S}{\sqrt{3}}\left(1 + \frac{\nu_1}{2} - \frac{\nu_2}{3}\right).$$

Allowing for (C.8b) we obtain

$$E_C \approx \frac{2\alpha D_S}{3\sqrt{3}}\left(1 - \frac{2\alpha^2R^2}{3(\alpha_R-\alpha)^2} + \frac{9\beta\vartheta}{2(\alpha_R-\alpha)\alpha}\right). \tag{C.9}$$

Let us rewrite the approximate formulas (C.4), (C.6) and (C.9) in the dimensionless variables R, $\vartheta/(\alpha D_S^2) = gR^2$ and $\xi = \alpha_R/\alpha$ ($\alpha < 0$, $\alpha_R \geqslant 0$, see also (18)), as follows:

$$D_r \approx D_S\sqrt{1 - \frac{gR^2}{1-\xi/3}}, \qquad \varepsilon_r \approx \frac{-1/2\alpha}{1 - [gR^2/(1-\xi/3) - [gR^2/(1-\xi/3)^2]}, \tag{C.10}$$

$$E_C \approx \frac{2\alpha D_S}{3\sqrt{3}}\left(1 - \frac{2R^2}{3(1-\xi)^2} - \frac{9gR^2}{2(1-\xi)}\right). \tag{C.11}$$

Comparing the approximate formulas (C.11) and (C.12) with the numerical calculations based on (18) at $\omega \to 0$, i.e. on (C.3), (C.5) and (C.7), we obtain that (C.10)–(C.12) are valid for $R < 1$, $\xi < -5$, $g > 5$ with 10% accuracy (e.g. see figure 3). Moreover, the following estimations are valid

$$|E_C| \approx \frac{2|\alpha D_S|}{3\sqrt{3}}\left(1 - \frac{3gR^2}{(1-\xi)}\right)^{3/2}, \qquad \varepsilon_r \approx \frac{1}{-2\alpha(1 - gR^2/(1-\xi/3))}. \tag{C.12}$$

References

[1] Burfoot J C and Taylor G W 1979 *Polar Dielectrics and their Applications* (London: Macmillan)
[2] Lines M E and Glass A M 1978 *Principles and Applications of Ferroelectrics and Related Phenomena* (Oxford: Oxford University Press)
[3] Smolensky G A *et al* 1984 *Ferroelectrics and Related Materials* (New York: Gordon and Breach)
[4] Landauer R 1957 *J. Appl. Phys.* **28** 227–34
[5] Bratkovsky A M and Levanyuk A P 2000 *Phys Rev. Lett.* **85** 4614–7
[6] Janovec V 1959 *Czech. J. Phys.* **9** 468

[7] Shimizu M, Nakashima S, Kaibara K, Fujisawa H and Niu H 2000 *Ferroelectrics* **241** 183–90
[8] Contreras J R, Kohlstedt H, Poppe U, Waser R and Buchal Ch 2003 *Appl. Phys. Lett.* **83** 126–8
[9] Shur V Ya, Rumyantsev E L, Makarov S D, Ponomarev N Yu, Nicolaeva E V and Shishkin E I 1999 *Integrated Ferroelectrics* **27** 179–94
[10] Hashimoto S, Orihara H and Ishibashi Y 1994 *J. Phys. Soc. Japan* **63** 1601–10
[11] Haken H 1978 *Synergetics* (Berlin: Springer)
[12] Jaffe B, Cook W R and Jaffe H 1971 *Piezoelectric Ceramics* (London: Academic)
[13] Cross L E 1991 *Ferroelectric Ceramics: Tailoring Properties for Specific Application* (Basel: Birkhauser)
[14] Glinchuk M D, Eliseev E A, Stephanovich V A and Fahri R 2003 *J. Appl. Phys.* **93** 1150–9
[15] Glinchuk M D and Morozovska A N 2004 *J. Phys.: Condens. Matter* **16** 3517
[16] Lo V C 2003 *J. Appl. Phys.* **94** 3353–9
[17] Pike G E, Warren W L, Dimos D, Tuttle B A, Ramesh R, Lee J, Keramidas V G and Evans J T 1995 *Appl. Phys. Lett.* **66** 484–6
[18] Bolten D, Bottinger U, Schneller T, Grossmann M, Lohse O and Waser R 2001 *Integrated Ferroelectrics* **32** 93–9
[19] Lebedev M and Akedo J 2002 *Japan J. Appl. Phys.* **41** 6669
[20] Haccart T, Soyer C, Cattan E and Remiens D 2001 *Ferroelectrics* **254** 185–93
[21] Cross L E 1987 *Ferroelectrics* **76** 241–5
[22] Granzow T, Dorfler U, Woike Th, Wohlecke M, Pankrath R, Imlau M and Kleemann W 2001 *Phys. Rev.* B **63** 174101(7)
[23] Gao Y, Uchino K and Viehland D 2002 *J. Appl. Phys.* **92** 2094–9
[24] Tamura T, Matsuura K, Ashida H, Konda K and Otani S 1999 *Appl. Phys. Lett.* **74** 3395–7
[25] Jiang Q Y, Subbarao E C and Cross L E 1994 *J. Appl. Phys.* **75** 7433–43
[26] Westphal V, Kleemann W and Glinchuk M D 1992 *Phys. Rev. Lett.* **68** 847–50
[27] Fridkin V M 1980 *Ferroelectrics Semiconductors* (New York: Consultant Bureau)
[28] Shklovskii B I and Efros A L 1984 *Electronic Properties of Doped Semiconductors* (Berlin: Springer)
[29] Shik A Y 1995 *Electronic Properties of Inhomogeneous Semiconductors* (New York: Gordon & Breach)
[30] Guro G M, Ivanchik I I and Kovtonuk N F 1968 *Fiz. Tverd. Tela* **10** 134–43 [*Sov. Phys.—Solid State* **10** 100–9]
[31] Kirsh B, Schmitt H and Muser H 1986 *Ferroelectrics* **68** 275–84
[32] Miller R C and Weinreich G 1960 *Phys. Rev.* **117** 1460–6
[33] Cao W and Cross L E 1991 *Phys. Rev.* B **44** 5
[34] Morozovska A N and Eliseev E A 2004 http://arXiv.org/cond-mat/0406296
[35] Morozovska A N, Eliseev E A and Obukhovsky V V 2004 *Ferroelectrics* **298** 257–70
[36] Zhirnov V A 1959 *Sov. Phys.—JETP* **35** 822–7
[37] Pertsev N A, Zembilgotov A G and Tagantsev A K 1998 *Phys. Rev. Lett.* **80** 1988–91
[38] Kittel C 1956 *Introduction to Solid State Physics* (London: Chapman & Hall)
[39] Darlindton C N W and Cernik R J 1991 *J. Phys.: Condens. Matter* **3** 4555
[40] Landau L D and Lifshitz E M 1998 *Statistical Physics. Theoretical Physics* vol 5 (Oxford: Butterworth-Heinemann)